DALHOUSIE UNIVERSITY

The explicit examination of the magnetic states of electrides

Stephen G. Dale[1, a)] and Erin R. Johnson[2, b)]

[1)] *Chemistry and Chemical Biology, School of Natural Sciences, University of California, Merced, 5200 North Lake Road, Merced, California 95343, USA*

[2)] *Department of Chemistry, Dalhousie University, 6274 Coburg Rd, P.O.Box 15000 B3H 4R2, Halifax, Nova Scotia, Canada*

(Dated: 9 September 2016)

Electrides are a unique class of ionic solids in which the anions are stoichiometrically replaced by electrons localised within the crystal voids. In this work, we present the first density-functional calculations to successfully reproduce the known anti-ferromagnetic behaviour of the organic electrides. Interrogation of the spin densities confirms that the localised, interstitial electrons are indeed the source of magnetism in the electride crystals. Comparison of the relative energies of the ferromagnetic and anti-ferromagnetic states allows prediction of the spin-coupling constants between electrons in neighbouring crystal voids. All major discrepancies between the calculated and experimentally-determined coupling constants reflect obvious deviations from the assumption of a simple, one-dimensional chain of interacting spins. For the electrides where such a model Hamiltonian is valid, the experimental ordering of the coupling constants is reproduced to a remarkable degree of accuracy.

[a)] Electronic mail: sdale@ucmerced.edu

[b)] Electronic mail: erin.johnson@dal.ca

I. INTRODUCTION

Electrides are ionic materials in which the anion is stoichiometrically replaced with localised electrons. The localised electrons result in a number of exotic properties which allow for many potential applications; existing examples are improved cathodes for fluorescent lights,[1] organic-light emitting diodes,[2] improved catalysts for CO_2[3] and N_2[4–6] splitting, in electrochemical reactions,[7] and as powerful, selective reducing agents.[8–11] So far, none of the existing applications take advantage of the magnetic properties of electrides.

The magnetic state of each of the known electrides has been measured experimentally using electron paramagnetic resonance (EPR) spectroscopy[12–17] and superconducting quantum interference devices (SQUID).[14? –19] EPR takes advantage of the Zeeman effect to measure the magnetic properties[?] of a material while SQUID takes advantage of the Josephson effect.[?] Both methods are capable of measuring the magnetic susceptibility of a material at varying temperatures to determine a material's magnetic behaviour. The electrides are consistently found to be anti-ferromagnetic and typically match Curie-Weiss behaviour at higher temperatures.[12–18] The origin of this anti-ferromagnetic behaviour is hypothesised to be the localised electrons, which interact with each other though narrow channels within the electride crystal structure. It is the theoretical reproduction of these magnetic properties that is the primary concern of this work.

Alternatively the magnetic behaviour of a material can be quantified by the spin-coupling constant. The coupling constant is a component of the Heisenberg Hamiltonian and describes the strength of the interaction between electrons at neighbouring sites in a dimer or lattice. A Heisenberg Hamiltonian can be chosen to match the geometry of the magnetic crystal and then a coupling constant determined such that the magnetic behaviour predicted by the Heisenberg Hamiltonian matches the magnetic susceptibility behaviour observed by the EPR and SQUID measurements. The Heisenberg Hamiltonian is particularly useful when experimentally examining magnetic behaviour as is allows for direct comparison with computationally determined coupling constants.

The particular form of the Heisenberg Hamiltonian, $\hat{H}$, is chosen depending on the geometry of the crystal voids within each electride. $Cs^+(15C5)_2e^-$, $Cs^+(18C6)_2e^-$, and Na^+(tri-pip-aza-2.2.2)e^- contain linear chains of crystal voids linked by major channels. Conse-

quently these electrides were modelled using the following 1D Heisenberg Hamiltonian:

$$\hat{H} = -2J \sum_i \hat{S}_i \bullet \hat{S}_{i+1} \tag{1}$$

where $\hat{S}_i$ is the spin operator for an electron at site i. J is the spin-coupling constant, which is typically positive for anti-ferromagnetic states and negative for ferromagnetic states. This Hamiltonian assumes that the electrons couple only with their nearest neighbours within a 1D chain and that the magnetic electron is localised within the electride crystal void.[12,15,20] Li^+(cryptand-2.1.1)e^- and Rb^+(cryptand-2.2.2)e^- contain zig-zag shaped channels and were also modeled using the 1D Heisenberg Hamiltonian, but may involve more complex electron coupling behaviour, which will be discussed in greater detail as it becomes relevant in Section III D.

A limitation of this analysis is that the chosen Hamiltonian does not necessarily reflect the true behaviour of the coupling in a given electride crystal. The most obvious example of this is K^+(cryptand-2.2.2)e^-, which could not be treated with the simple 1D model and required an alternating linear-chain Heisenberg Hamiltonian due to its 2D connectivity.[12] Also, description of the unique cyclic geometry of the crystal voids in $[Cs^+(15C5)(18C6)e^-]_6(18C6)$ required the use of a six-membered Heisenberg ring Hamiltonian.[19]

Theoretical studies of electrides have typically focused on demonstrating and quantifying the presence of localised electrons,[12,21–36] This supplements experimental investigations, which can only infer the presence of localised electrons.[20,37,38] More recent theoretical work has focused on examining the properties of electride crystals[39**?** –44] and proposing new electrides by examining crystallographic databases[6,36,45–47] or using new electride design philosophies.[33,39,48–70]

To date, there is only one study, by Ryabinkin *et al.*,[42] that reproduces the expected magnetic properties of electride crystals. The theoretical model is based on two interacting 'particles in a box', treated with an exact two-electron Hamiltonian.[71,72] The 'box' consists of two spheres, intended as the crystal voids in which electrons will localise, connected by a channel through which the electrons interact. Using this appropriately coined 'dog-bone' model, Ryabinkin and Staroverov were able to reproduce the predicted geometry-dependent magnetic-susceptibility behaviour proposed by Dye[12] They then proceeded to suggest a modified relationship between crystal geometry and magnetic susceptibility that is even more consistent with existing electride data.

Our previous density-functional study[32] of the eight known electrides (at that time), attempted to account for magnetic behaviour by including spin polarisation in the density functional treatment. The typical method for examination of a particular magnetic state is to assign a magnetic bias to one or more atoms within the crystal. However, as the localised electron is not associated with an atom, it is unclear where to place the initial magnetic bias. In our previous work, the magnetic bias was placed on the alkali-metal atoms, the ionisation of which is the source of the localised electrons. While this allowed us to treat all of the electrides in the same manner, it also placed the magnetic bias as far from the localised electron as possible. A ferromagnetic state was identified for $Cs^+(15\text{-crown-}5)_2e^-$ using this method, but despite multiple attempts to obtain other, similar magnetic states, only non-magnetic, closed-shell solutions were found for the remaining electrides. Although the inability to include magnetic properties in this initial study was frustrating, it was not a major hindrance to the extraction of new and insightful information regarding the electronic structure of electrides. It will be seen that the previous conclusions regarding quantification of the localised electron are reinforced by the more sophisticated magnetic-state calculations presented herein.

FIG. 1: The structure of the $Cs^+(15\text{-crown-}5)_2e^-$ electride.[18] The green sphere represents the localised electron within the crystal void. The initial magnetic bias is assigned to the nearest hydrogen atoms, highlighted as teal.

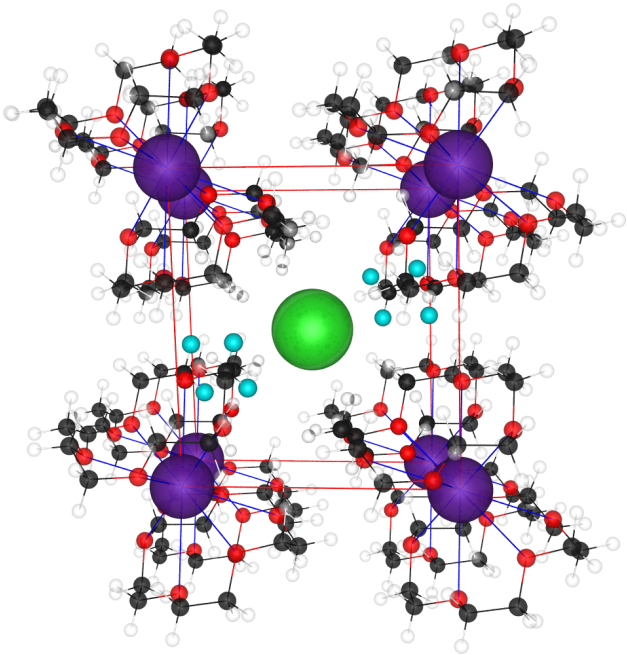

This work presents the first magnetic-state description of the organic electrides using density-functional theory (DFT). A far more successful approach to obtaining magnetic states is to apply a magnetic bias to hydrogen atoms neighbouring the crystal void. Figure 1 shows the crystal structure of the simplest organic electride, $Cs^{+}(15\text{-crown-}5)_2e^{-}$, with the eight hydrogen atoms closest to the localised-electron centre (green) highlighted teal. It is these eight hydrogen atoms to which an initial magnetic bias is applied. While these hydrogen atoms are clearly not the origin of the magnetic properties of electrides, this is a much closer initial approximation to the desired final state than is our previous choice of the alkali metal atoms (purple). This new approach to assigning the initial magnetic bias is only applicable to the organic electrides, as the inorganic electrides[6,36,45,46] do not contain hydrogen atoms and are not considered here. By moving the initial magnetic bias from the alkali metal to the hydrogen atoms, magnetic states were obtained for six of the seven organic electrides. These new solutions are compared to previous non-magnetic DFT results, specifically examining the differences between each description. Comparison is also made with experimental magnetic data, specifically spin-coupling constants determined from EPR measurements.

II. COMPUTATIONAL METHODS

Density-functional calculations on the seven known organic electrides were performed using geometries taken directly from the experimental crystal structures. Any modification of the known crystal structures was identical to our previous work.[32] Periodic boundary conditions were applied using the planewave/pseudopotential (PW/PS) approach and the Projector Augmented Wave (PAW) formalism[73] with the Quantum Espresso program.[74] Single-point spin-polarised and unpolarised calculations for each electride were conducted to find the ferromagnetic and non-magnetic, closed-shell solutions, respectively. The PBE functional[75] was used, with a cut-off energy of 50 Ry with cold smearing[76] at a smearing temperature of 0.01 Ry.

The primary change from our previous work is the choice of the initial magnetic bias assigned in the spin-polarised calculations. In this work, up to eight hydrogen atoms closest to the localised electron were given an initial magnetic bias; an example of this is provided in Figure 1. The location of the localised electron is taken to correspond to the coordinates

of the major non-nuclear maxima (NNM) found from QTAIM analysis of the closed-shell electron density, performed using the critic2 program.[77,78] QTAIM analysis, with the Yu-Trinkle[79] integration algorithm, was also used to calculate the amount of charge localised within the crystal void of each electride. This allows for a quantitative comparison of the extent of electron localisation for each of the magnetic states. Assigning a magnetic bias to an atom causes a renormalisation of of the atomic spin densities of that atom which is then used to construct the initial self-consistent field (SCF) guess. In Quantum Espresso a magnetic bias of $+1$ causes all of the electrons associated with an atom to be α-spin rather than β-spin, and this is reversed for a magnetic bias of -1. Absolute magnetic biases less that 1 allow for fractional assignment of α and β spin occupation. Closed-shell calculations use an initial guess with no magnetic bias, so the numbers of α- and β-spin electrons, and hence the atomic densities for each spin, are equal.

The initial magnetic bias is replicated for each periodic image. Consequently, calculations using a single electride unit-cell give the correct ferromagnetic solution, but can frequently result in either no anti-ferromagnetic solution, or a non-optimal one. In order to fully and reliably explore anti-ferromagnetic states, the unit-cells for a subset of the electrides were replicated to create a super-cell in which opposite-spin electrons neighbour each other. The simplest example of this is Cs^+(15-crown-5)$_2e^-$, which contains a single localised electron and hence always converges to either a ferromagnetic or non-magnetic, closed-shell solution. To find the anti-ferromagnetic solution, the Cs^+(15-crown-5)$_2e^-$ unit-cell needs to be replicated in the x, y, and z directions, with an alternating (G-type) magnetic bias given to the hydrogen atoms in neighbouring unit-cells. Clearly this significantly increases the size of the calculation as an initial unit-cell with 71 atoms becomes a 568-atom super-cell. As a further example, since the unit-cell of Cs^+(18-crown-6)$_2e^-$ contains two localised electrons, it must only be replicated in the x and y directions to generate an appropriate spin-oriented anti-ferromagnetic state. The ordering of all of the anti-ferromagnetic states in this work is G-type with the exception of $[Cs^+(15C5)(18C6)e^-]_6(18C6)$ which will be discussed in greater detail in Section III D. Table I gives the number of unit-cell replications required to achieve anti-ferromagnetic solutions for each electride, in addition to the number of $\boldsymbol{k}$-points used and other relevant structural information.

One organic electride, K^+(cryptand-2.2.2)e^-, is not included in Table I as we were still unable to find a magnetic solution for this compound with the new magnetic bias assign-

TABLE I: List of the electride crystals considered and their corresponding Cambridge Structural Database[80] (CSD) codes. The number of unit-cell replications required to obtain an anti-ferromagnetic state, as well as the resulting total numbers of atoms and of localised electrons, and the $\boldsymbol{k}$-point mesh used in the calculations, are also given. The mCn notation stands for the m-crown-n ether molecule.

Electride	CSD Code	Unit-cell Replications	No. Atoms	No. Localised Electrons	$\boldsymbol{k}$-points (k×k×k)
$Cs^+(15C5)_2e^-$	TAGFEM	8	586	8	1
$Cs^+(18C6)_2e^-$	DUBCIM	4	680	8	1
$[Cs^+(15C5)(18C6)e^-]_6(18C6)$	WIHFIC†	1	510	6	1
Rb^+(cryptand-2.2.2)e^-	EBEWOX	1	126	2	4
Na^+(tri-pip-aza-2.2.2)e^-	DAWCIO	1	324	4	2
Li^+(cryptand-2.1.1)e^-	ROGDAS	1	196	4	4

† this electride actually requires 8 unit-cell replications to obtain a proper anti-ferromagnetic state. As this would involve over 4080 atoms, our calculations are limited to the single unit-cell. This is discussed further in Section III D.

ment. The cavity-channel structure of K^+(cryptand-2.2.2)e^- is uniquely open, with elongated crystal voids and 2D connectivity.[12,28,38] This has led to speculation that electron pairs are trapped within each crystal void, as opposed to individual, unpaired electrons. Further its magnetic susceptibility can only be modelled by an alternating-linear-chain Heisenberg Hamiltonian rather than the usual linear Heisenberg Hamiltonian (this will be discussed in greater detail in Section III D). Clearly K^+(cryptand-2.2.2)e^- is a complex electride and the simple approach used here to find the magnetic states of the other electrides is not sufficient in this case.

Since spin symmetry must be broken to obtain anti-ferromagnetic solutions for the electrides, these calculations will not correspond to pure-spin states and may be subject to spin contamination. One benefit of using PBE in the present work is that such pure density functionals are the most reliable single-reference methods for treating spin-mixed states. These functionals minimize both spin contamination and errors arising from neglect of multi-center, or static, electron correlation.[81,82] Other computational methods beyond DFT are capable of

describing static correlation and maintaining spin-pure states to varying degrees of success, with multi-reference methods being the most reliable,[83–87] although they are prohibitively expensive computationally. For broken-symmetry calculations using single-reference methods, spin-projection has been suggested for acquisition of spin-pure states.[88–93] However, these methods are impractical when considering the size and periodic nature of the electride crystals that are the subject of this work.

To identify the origin of the magnetic behaviour in the electride crystals, we calculate and plot the difference between the α and β electron densities. Closed-shell solutions will uniformly give zero for this value. However the imbalances in spin distribution for both the ferromagnetic and anti-ferromagnetic states are obvious and are shown in Figure 2. The other visualisation methods[94–97] used in our previous work[32] do not contribute significant new information. In particular, the procrystal density of the electrides is determined purely based on geometry and free-atomic electron densities, and therefore provides identical results, regardless of the choice of calculation method. Conversely, non-covalent interaction (NCI) plots[98,99] are dependent on the DFT electron density and serve as a valuable reality check. The NCI plots generated using the electron densities from the ferromagnetic states are almost indistinguishable from those generated using non-magnetic, closed-shell densities.

It is worth noting here that the present calculations were deliberately performed with the final, G-type magnetic states in mind, which introduces a bias to our results. However, when alternative types of magnetic ordering were found they were consistently higher in energy than the G-type solution. Thus, this approach seems to identify the optimal magnetic ground states available to the electride crystals, within the confines of the calculations conducted.

III. RESULTS AND DISCUSSION

A. Spin Densities and Magnetisations

The magnetic states in the electride crystals are hypothesised to be caused by coupling between the localised electrons.[28] Magnetic states must have local imbalances in the electronic spin density. As such, closed-shell calculations, which assume equivalent densities for each spin, will never predict magnetic states. For spin-polarised solutions, the location of the spin imbalance and the origin of the overall magnetic behaviour can be identified from

FIG. 2: The spin density of the organic electrides in the ferromagnetic (left) and anti-ferromagnatic states (right). The blue and red surfaces, corresponding to α and β spin densities, are plotted using +0.001 and -0.001 au iso-surface values, respectively.

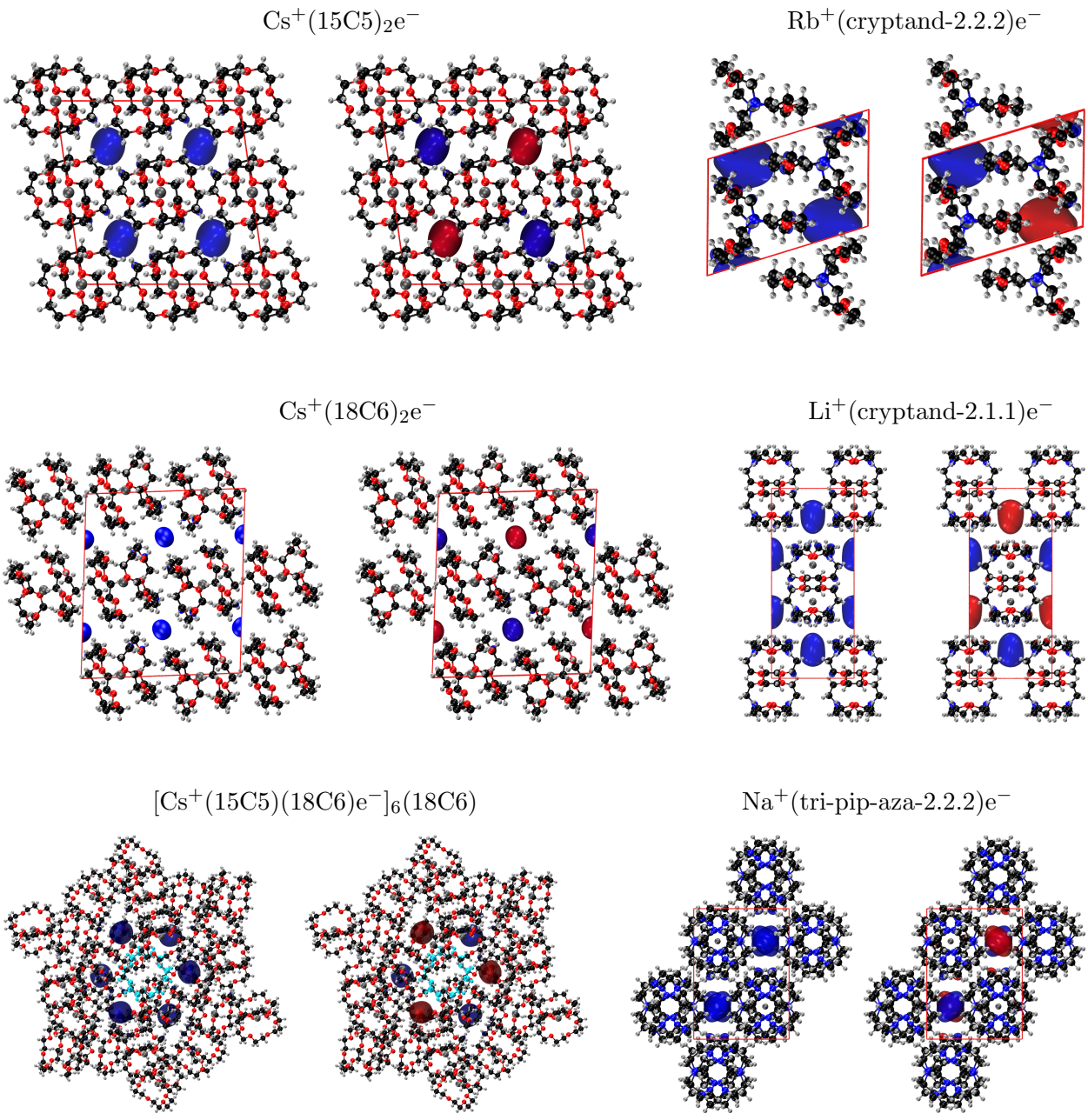

plots of the spin-density difference. Such plots are shown in Figure 2 for both ferromagnetic and anti-ferromagnetic states of all six electrides considered, using a density iso-surface value of 0.001 au. This representation allows for visualisation of the unpaired-spin regions within the electride crystals.

Satisfyingly, the electrides for which magnetic states are found all show a spin imbalance within the crystal void. This is consistent with the regions identified in our previous work to contain localised electrons, even leaving out the small extra crystal voids present in $[Cs^+(15C5)(18C6)e^-]_6(18C6)$.[32] This confirms that the magnetism observed in electrides is caused by the localised electrons.

TABLE II: Calculated total and absolute spins, per localised electron, for the ferromagnetic and anti-ferromagnetic states of each electride. Total spin represents the integral of the difference between the α and β spin densities, while the absolute spin represents the integral of the absolute value of the spin-density difference. The absolute and total spin of the non-magnetic, closed-shell states is by definition zero.

	Ferromagnetic		Anti-ferromagnetic	
Electride	Total Spin	Absolute Spin	Total Spin	Absolute Spin
$Cs^+(15C5)_2e^-$	0.92	0.93	0.00	0.87
$Cs^+(18C6)_2e^-$	0.86	0.86	0.00	0.79
$[Cs^+(15C5)(18C6)e^-]_6(18C6)$	0.89	0.90	0.00	0.87
Rb^+(cryptand-2.2.2)e^-	0.91	0.92	0.00	0.85
Na^+(tri-pip-aza-2.2.2)e^-	0.89	0.90	0.00	0.86
Li^+(cryptand-2.1.1)e^-	0.82	0.82	0.00	0.78

The total and absolute spin polarizations for both magnetic states of each electride are reported in Table II and are normalized by dividing by the total number of localised, interstitial electrons, as given in Table I. For the non-magnetic, closed-shell state, both of these quantities are zero by definition. For pure spin states, the absolute spin should equal the number of localised electrons and each result approaches the expected integer value. The total spins reflect either the spin alignment characteristic of ferromagnetic states or the balanced spins characteristic of anti-ferromagnetic states.

B. Interstitial Charge

The positions of the non-nuclear maxima (NNM) in the electron density were identified for all the magnetic states found. The integral of the density within the QTAIM basin

corresponding to the NNM can be interpreted as the amount of localised charge. The NNM charge per localised electron is provided in Table III for the spin-polarized and closed-shell states of each electride. As in our previous work we observe fractional electron localisation within the crystal voids, consistent with similar studies on solvated electrons in water.[33,100,101] While the amount of localised charge would be expected to increase upon the inclusion of exact exchange,[102,103] the use of appropriate hybrid functionals is untenable for systems of this size.

TABLE III: Calculated QTAIM charges for the NNM basins, per localised electron, for three magnetic states of each electride.

Electride	Anti-ferromagnetic State Charge	Ferromagnetic State Charge	Spin-Restricted state charge
$Cs^+(15C5)_2e^-$	0.362	0.361	0.273
$Cs^+(18C6)_2e^-$	0.362	0.356	0.273
$[Cs^+(15C5)(18C6)e^-]_6(18C6)$	0.291	0.291	0.183
Rb^+(cryptand-2.2.2)e^-	0.333	0.330	0.249
Na^+(tri-pip-aza-2.2.2)e^-	0.282	0.282	0.196

Significant changes in the amount of localised charge are observed depending on the spin configuration. In all cases shown in Table III, the amount of localised charge increases when the electron density is spin-polarised. This effect is caused because electron-density maxima that should correctly correspond to a single, unpaired spin are reduced in magnitude for the equivalent closed-shell solutions, thus reducing the overall charge associated with each NNM. For the non-magnetic, closed-shell configuration, non-dynamical correlation[?] between opposite-spin electrons should serve to further localise the electron density in the interstitial regions. However, local density functionals such as PBE neglect non-dynamical correlation,[?] causing lower density values and broader density distributions for the localised electrons, relative to the spin-polarized calculations.

Li^+(cryptand-2.1.1)e^- is not shown in Table III as NNM are not observed for the spin polarised states. We verified this result using calculations with increased cut-off energies and found NNM in some cases and no NNM at all in others. To investigate the cause of these transient NNM in Li^+(cryptand-2.1.1)e^- we plotted the electron density along the x,

y, and z directions, with the origin taken as the location of the NNM in our previous non-magnetic, closed-shell calculations.[32] These plots, included in the Supporting Information, show a density maxima in the x and z directions but an electron density shoulder in the y direction. The sensitivity of the QTAIM analysis is likely due to small changes in the shape of this flat shoulder. This reiterates a point we have previously made,[32] which is that NNM are not necessarily a requirement for electron localisation and electride-like behaviour, as was the case for $[Ca_{24}Al_{28}O_{68}]^{4+}4e^-$. Further, if we compare density plots of the closed-shell and spin-polarised calculations we do still see an increase in electron density at the putative NNM point, consistent with Table III.

C. Relative Stabilities

For all of the electrides considered, the anti-ferromagnetic configuration is the most stable. This is consistent with the single-crystal EPR experiments conducted on electrides[12–20] and the models proposed by Dye[12] and Ryabinkin and Staroverov,[42] all of which predict anti-ferromagnetic behaviour.

TABLE IV: Energies of the ferromagnetic and non-magnetic, closed-shell states, relative to the anti-ferromagnetic state, for each electride, (in kJ/mol per localised electron). The calculated and experimentally-determined coupling constants (in K) are also reported. The order of the table has been changed to reflect the increasing magnitude of the experimental coupling constants.

Electride	Ferromagnetic State Energy	Closed-shell State Energy	Coupling Constant Computational	Coupling Constant Experimental
$Cs^+(15C5)_2e^-$	0.2036	2.9480	12.2	3[12]
Na^+(tri-pip-aza-2.2.2)e^-	0.2559	2.3966	15.4	11.1[20]
Rb^+(cryptand-2.2.2)e^-	0.7115	5.6985	78.2	30[15]
$Cs^+(18C6)_2e^-$	0.4428	1.9483	26.6	38[12]
Li^+(cryptand-2.1.1)e^-	1.4715	2.4651	177.0	54[12]
$[Cs^+(15C5)(18C6)e^-]_6(18C6)$	0.2529	2.6689	15.2	410[19]

Table IV reports the energies, per localised electron, of the non-magnetic, closed-shell and

ferromagnetic states of each of the electrides, relative to the anti-ferromagnetic state. The non-magnetic, closed-shell states are consistently much higher in energy than either of the magnetic states. This is because closed-shell calculations require the α and β spin densities to be equal and do not account for multi-reference character, arising from the mixing of degenerate electronic states. The elevated energies observed for the closed-shell solutions are a consequence of the missing static-correlation component of the energy that is absent from closed-shell solutions.

An alternative interpretation of static-correlation error is provided by Cohen *et al.*[81] In that work, an ensemble picture enables the mixing of degenerate electronic configurations to be represented by fractionally changing the spin of a single electron. In the correct density-functional treatment, the energy should remain constant as the fractional spin is varied between the integer values corresponding to each spin pure state. However, with all common density-functional methods, an energy maximum is observed whenever an electron is described as half α and half β spin. The analogue in our work is that the non-magnetic, closed-shell solutions describe the localised electrons as half α and half β spin, while they are represented as full α or β spins in the magnetic states. As a result, we observe an energy maxima for the closed-shell solutions, relative to the spin-polarised.

The calculations on the magnetic states were performed using spin-polarised methods, which do account for static-correlation effects from the mixing of degenerate electronic states (the simplest being inversion of the observed spin) by breaking spin symmetry. The anti-ferromagnetic state is an example of this, where the mixing of multiple states is required to give the broken-symmetry solutions shown in Figure 2. However, this state mixing leads to spin contamination and non-ideal spin-quantum numbers. It is clear that some spin contamination is present in all the magnetic-state calculations found in this work upon consultation of Table II, since spin-pure states should always give integer magnetisation values. However, the resulting energies provide reasonable coupling constants, as we will see in the following section.

D. Coupling Constants

The results of our calculations, specifically the difference in energy between the ferromagnetic and anti-ferromagnetic states, can be converted to a coupling constant if a Heisen-

berg Hamiltonian is assumed. Our DFT calculations model all possible interactions within the super-cell; this causes complications when attempting to make comparisons with the experimentally-determined coupling constants, which assumed only 1D nearest-neighbour interactions. For these reasons, it is not obvious how to directly compare our DFT results with previous experimental studies. We choose the simplest solution and assume a 1D Heisenberg Hamiltonian, as was used in the determination of couplings from the experimental EPR and SQUID data.[12,15,20]

The solution to the infinite 1D Heisenberg Hamiltonian is equivalent to a pair of dimer interactions for each electron, one with each of its immediate neighbours. For two interacting atoms, each bearing a single, unpaired electron, the coupling constant can be determined from the energy difference between the triplet and singlet states.[104]

$$J = -\frac{1}{2}(E_T - E_S) \tag{2}$$

For the electrides, if the calculated energies are divided by the number of localised electrons in the super-cell, N, the coupling constant can be determined analogously, from the energy difference between the ferromagnetic and anti-ferromagnetic states.[42]

$$J = -\frac{1}{2N}(E_F - E_A) \tag{3}$$

Although the broken-symmetry anti-ferromagnetic solution from DFT does not strictly correspond to a pure spin state, it is not clear how to isolate pure spin-state energies from the DFT results.[84,105] As Table II shows that the magnetisations are close to the ideal integer values, this should be a reasonable approximation.

The calculated coupling constants are provided in Table IV, together with the corresponding experimental values. The result for $[Cs^+(15C5)(18C6)e^-]_6(18C6)$ shows the most significant deviation from the experimental coupling constant. This is because, as mentioned in Table I the calculated anti-ferromagnetic state does not correspond to the 'true' anti-ferromagnetic state expected for this electride. The crystal voids in $[Cs^+(15C5)(18C6)e^-]_6(18C6)$ contain channels that link to neighbouring crystal voids both inside and outside the unit-cell. If the unit-cell shown in Figure II is replicated, each localised electron will have a cross-cell neighbour of the same spin. This is illustrated in Figure 3, which shows only the NNM sites in $[Cs^+(15C5)(18C6)e^-]_6(18C6)$, with the same alternating spin arrangement shown in Figure II. The unit-cell is replicated in the x, y and z directions to highlight the nearest-neighbour interactions with adjacent unit-cells, each of which

are same-spin interactions. Hence, this is clearly not the most-stable anti-ferromagnetic state and the calculated coupling constant will be strongly underestimated relative to the experimental value. While replication of the unit-cell of $[Cs^+(15C5)(18C6)e^-]_6(18C6)$, as described in Section II, should give the correct anti-ferromagnetic solution, the super-cell required would contain 4080 atoms and this is currently an impractical calculation.

FIG. 3: The locations of the six NNM sites for the anti-ferromagnetic state of $[Cs^+(15C5)(18C6)e^-]_6(18C6)$ are represented using opaque red and blue spheres to indicate localised α-spin and β-spin electrons, respectively. The central unit-cell is repeated in the x, y and z directions, although the replica immediately behind the original unit-cell is omitted for clarity. The nearest neighbour interactions are highlighted, using purple for opposite-spin interactions and either red or blue for same-spin interactions.

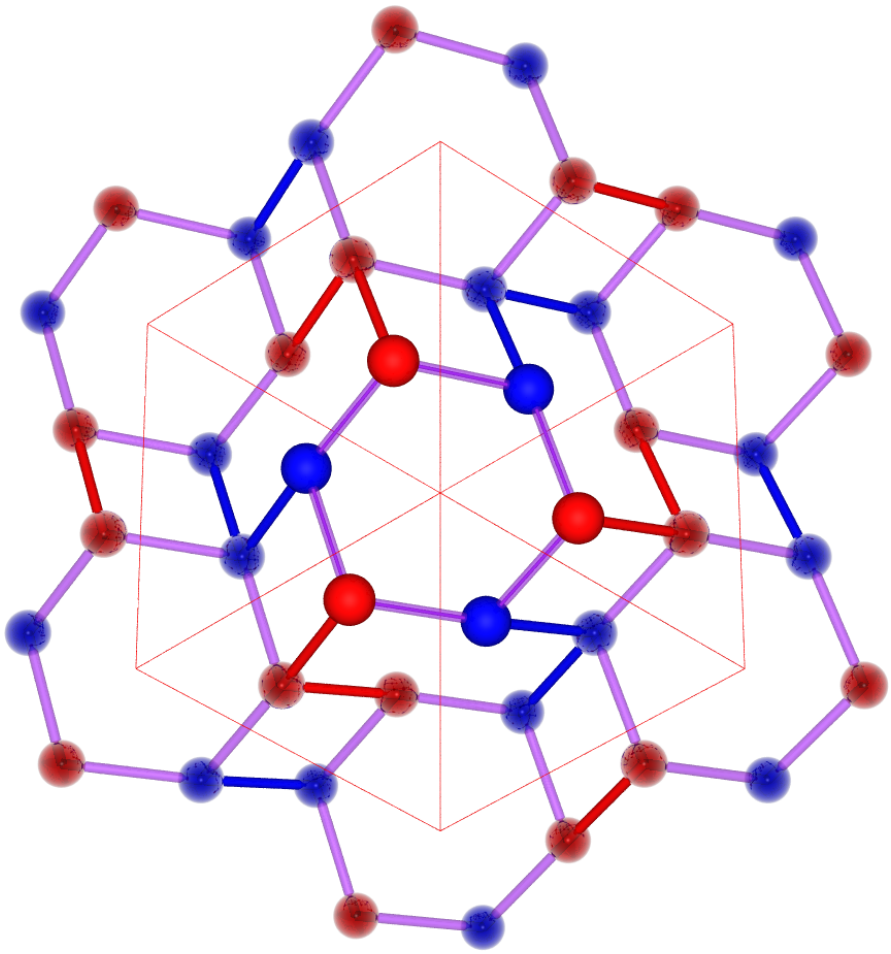

For the remaining electrides, the comparison between the calculated and experimental coupling constants are encouraging, with DFT roughly providing the correct ordering of

coupling constants. The largest differences between theory and experiment are for the coupling constants of Rb^+(cryptand-2.2.2)e^- and Li^+(cryptand-2.1.1)e^-. As mentioned in the introduction this is potentially due to the secondary channels in these two electrides which do not strictly follow the 1D Heisenberg Hamiltonian behaviour. While this is not obvious upon inspection of a single unit-cell, as shown in Figure 2, it becomes apparent when more than one unit-cell is considered, as in Figure 4 or figures contained in Refs. 12 and 15. Figure 4 provides NCI plots of Li^+(cryptand-2.1.1)e^- and Rb^+(cryptand-2.2.2)e^-, overlaid with the anti-ferromagnetic spin densities from Figure 2. The NCI plots highlight the channels through which the localised electrons interact. The panels on the left show the major channels for these interactions, in which the zig-zag paths between adjacent, opposite-spin electrons are clear. The panels on the right show a rotated view of each lattice, in which the major channels are now oriented vertically. By considering more than one unit-cell, this rotated orientation allows the smaller, minor channels between diagonally-neighbouring opposite-spin electrons to be seen as well. Thus, while the 1D Heisenberg Hamiltonian initially seems to be a reasonable approximation for such zig-zag lattices, it neglects the extra contributions to the coupling arising from the minor channels in these electrides.

Considering the complications regarding which model is most appropriate to calculate and compare magnetic coupling constants, our results are remarkably good. State-of-the-art DFT calculations on very simple intermolecular complexes typically provide errors in excess of 0.2 kcal/mol,[106] or 100 K. The present calculations treat much more complex systems, yet qualitatively reproduce the expected ordering of the coupling constants of the $Cs^+(15C5)_2e^-$, Na^+(tri-pip-aza-2.2.2)e^-, and $Cs^+(18C6)_2e^-$ electrides, for which the 1D model is most applicable and the values span a range of less than 40 K. We attribute this degree of accuracy to significant cancellation of errors as the differences in the electronic structure between the ferromagnetic and anti-ferromagnetic states are quite small. As our calculations employ identical crystal geometries for the two magnetic states, we expect the cancellation of errors to be even more advantageous than in typical regimes.[107] This is further reinforced by the fact that the calculated NNM charges in Table III show negligible differences between the ferromagnetic and anti-ferromagnetic states. Thus, other than the change in spin density, the differences in total electron density between these two magnetic states are negligible.

FIG. 4: NCI plots for Li^+(cryptand-2.1.1)e^- (top) and Rb^+(cryptand-2.2.2)e^- (bottom) overlaid with the anti-ferromagnetic spin density of each crystal, shown from two different perspectives. The blue and red surfaces, corresponding to α and β spin densities, are plotted using +0.001 and -0.001 au iso-surface values, respectively. The green iso-surface from the NCI plot corresponds to a reduced density gradient value of 0.5 au. The molecular structure is not shown for clarity.

Li^+(cryptand-2.1.1)e^-

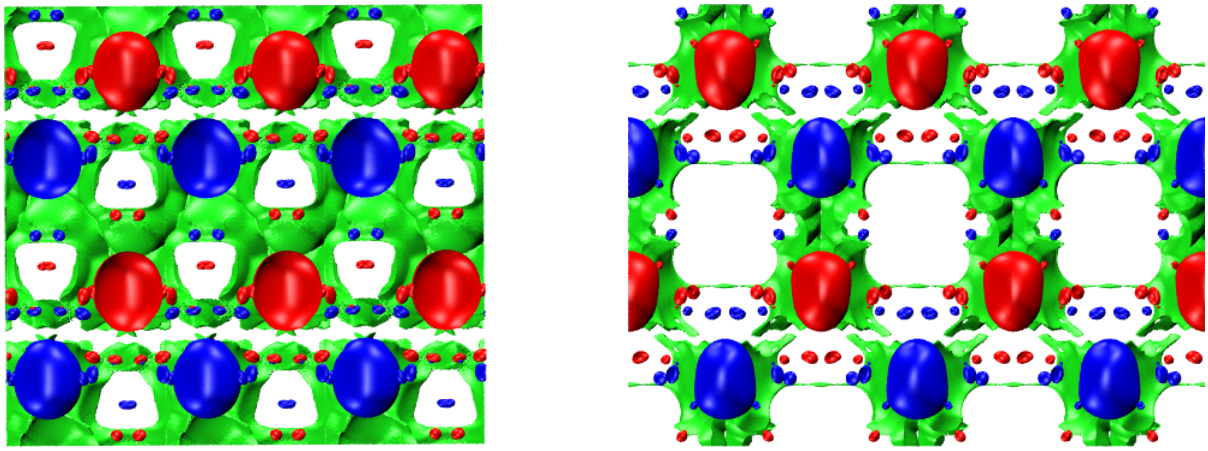

Rb^+(cryptand-2.2.2)e^-

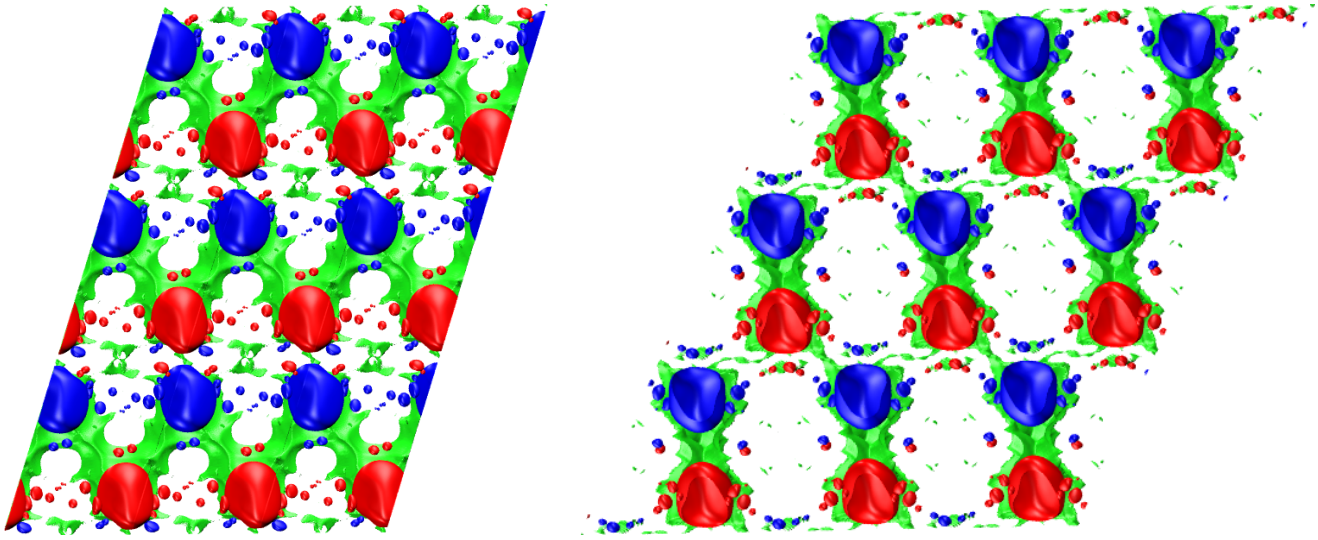

IV. CONCLUSIONS

We have demonstrated that it is possible to model magnetic states of the organic electride crystals using DFT methods. These magnetic states show local spin-density imbalances

within the electride crystal voids. This confirms that the magnetic character of electrides is indeed caused by coupling between the localised, interstitial electrons. Both the ferromagnetic and anti-ferromagnetic states show increased electron density within each crystal void, corresponding to the non-nuclear density maxima, relative to non-magnetic, closed-shell solutions. This implies that the electrides possess even stronger electron-localising character than seen in previous work.[32]

The anti-ferromagnetic spin states are consistently found to be the most stable, in agreement with both the experimentally-observed anti-ferromagnetic character of the organic electride crystals and the theoretical 'dog-bone' model.[42] By assuming a 1D Heisenberg model, we were able to determine spin-coupling constants to a remarkable degree of accuracy, roughly reproducing the experimental ordering of the coupling strengths. The largest deviation from experimental coupling constants was $[Cs^+(15C5)(18C6)e^-]_6(18C6)$ for which a calculation necessary to attain a correct anti-ferromagnetic solution is impractical. Rb^+(cryptand-2.2.2)e^- and Li^+(cryptand-2.1.1)e^- also exhibited deviations from the expected coupling-strength ordering, likely due to the 1D Heisenberg model excluding contributions from the minor channels in the electride crystals.

Satisfyingly, these magnetic descriptions of the organic electride crystals reinforce the previous theoretical conclusions regarding electron localisation, while providing significant additional information regarding their electronic structure. Spin-polarised calculations and prediction of magnetic couplings provide a new computational tool to apply to the ongoing goal of new electride development.

V. ACKNOWLEDGEMENTS

We would like to thank Dr. Alberto Otero-de-la-Roza (The University of British Columbia, Okanagan), Dr. Lee M. Thompson (The University of California, Merced) and Luc LeBlanc (Dalhousie University) for helpful comments and discussions. We also thank the National Sciences and Engineering Research Council of Canada (NSERC) for financial support and the Multi-Environment Computer for Exploration and Discovery (MERCED) for computational time.

REFERENCES

[1]S. Watanabe, T. Watanabe, K. Ito, N. Miyakawa, S. Ito, H. Hosono, and S. Mikoshiba, Sci. Technol. Adv. Mat. **12**, 034410 (2011).

[2]H. Yanagi, K.-B. Kim, I. Koizumi, M. Kikuchi, H. Hiramatsu, M. Miyakawa, T. Kamiya, M. Hirano, and H. Hosono, J. Phys. Chem. C **113**, 18379 (2009).

[3]Y. Toda, H. Hirayama, N. Kuganathan, A. Torrisi, P. V. Sushko, and H. Hosono, Nature communications **4** (2013).

[4]M. Kitano, Y. Inoue, Y. Yamazaki, F. Hayashi, S. Kanbara, S. Matsuishi, T. Yokoyama, S.-W. Kim, M. Hara, and H. Hosono, Nature chemistry **4**, 934 (2012).

[5]M. Kitano, S. Kanbara, Y. Inoue, N. Kuganathan, P. V. Sushko, T. Yokoyama, M. Hara, and H. Hosono, Nature communications **6** (2015).

[6]Y. Lu, J. Li, T. Tada, Y. Toda, S. Ueda, T. Yokoyama, M. Kitano, and H. Hosono, J. Am. Chem. Soc. **138**, 3970 (2016).

[7]J. Li, B. Yin, T. Fuchigami, S. Inagi, H. Hosono, and S. Ito, Electrochem. Commun. **17**, 52 (2012).

[8]H. Buchammagari, Y. Toda, M. Hirano, H. Hosono, D. Takeuchi, and K. Osakada, Organic letters **9**, 4287 (2007).

[9]S. Choi, Y. J. Kim, S. M. Kim, J. W. Yang, S. W. Kim, and E. J. Cho, Nature communications **5** (2014).

[10]Y. J. Kim, S. M. Kim, H. Hosono, J. W. Yang, and S. W. Kim, Chemical Communications **50**, 4791 (2014).

[11]Y. J. Kim, S. M. Kim, E. J. Cho, H. Hosono, J. W. Yang, and S. W. Kim, Chemical Science **6**, 3577 (2015).

[12]J. L. Dye, Inorganic Chemistry **36**, 3816 (1997).

[13]M. J. Wagner, R. H. Huang, and J. L. Dye, J. Phys. Chem. **97**, 3982 (1993).

[14]R. H. Huang, M. J. Wagner, D. J. Gilbert, K. A. Reidy-Cedergren, D. L. Ward, M. K. Faber, and J. L. Dye, J Am. Chem. Soc. **119**, 3765 (1997).

[15]Q. Xie, R. H. Huang, A. S. Ichimura, R. C. Phillips, W. P. Pratt, and J. L. Dye, J. Am. Chem. Soc. **122**, 6971 (2000).

[16]M. J. Wagner, A. S. Ichimura, R. H. Huang, R. C. Phillips, and J. L. Dye, J. Phys. Chem. B **104**, 1078 (2000).

[17]S. Matsuishi, Y. Toda, M. Miyakawa, K. Hayashi, T. Kamiya, M. Hirano, I. Tanaka, and H. Hosono, Science **301**, 626 (2003).

[18]S. B. Dawes, J. L. Eglin, K. J. Moeggenborg, J. Kim, and J. L. Dye, J. Am. Chem. Soc. **113**, 1605 (1991).

[19]M. Wagner and J. Dye, J. Solid State Chem. **117**, 309 (1995).

[20]M. Y. Redko, J. E. Jackson, R. H. Huang, and J. L. Dye, J. Am. Chem. Soc. **127**, 12416 (2005).

[21]G. Allan, M. De Backer, M. Lannoo, and I. Lefebvre, Europhys. Lett. **11**, 49 (1990).

[22]R. Rencsok, T. Kaplan, and J. Harrison, J. Chem. Phys. **93**, 5875 (1990).

[23]S. Golden and T. R. Tuttle Jr, Phys. Rev. B **45**, 13913 (1992).

[24]D. Singh, H. Krakauer, C. Haas, and W. Pickett, (1993).

[25]R. Rencsok, T. A. Kaplan, and J. F. Harrison, J. Chem. Phys. **98**, 9758 (1993).

[26]T. Kaplan, R. Rencsok, and J. Harrison, Phys. Rev. B **50**, 8054 (1994).

[27]S. Golden and T. R. Tuttle Jr, Phys. Rev. B **50**, 8059 (1994).

[28]J. L. Dye, M. J. Wagner, G. Overney, R. H. Huang, T. F. Nagy, and D. Tomanek, J. Am. Chem. Soc. **118**, 7329 (1996).

[29]P. V. Sushko, A. L. Shluger, K. Hayashi, M. Hirano, and H. Hosono, Phys. Rev. Lett. **91**, 126401 (2003).

[30]Z. Li, J. Yang, J. Hou, and Q. Zhu, Angew. Chem. Int. Edit. **43**, 6479 (2004).

[31]P. V. Sushko, A. L. Shluger, M. Hirano, and H. Hosono, J. Am. Chem. Soc. **129**, 942 (2007).

[32]S. G. Dale, A. Otero-de-la Roza, and E. R. Johnson, Phys. Chem. Chem. Phys. (2014).

[33]B. G. Janesko, G. Scalmani, and M. J. Frisch, J. Chem. Phys. **141**, 144104 (2014).

[34]M.-S. Miao and R. Hoffmann, Accounts of chemical research **47**, 1311 (2014).

[35]M.-s. Miao and R. Hoffmann, Journal of the American Chemical Society **137**, 3631 (2015).

[36]Y. Zhang, Z. Xiao, T. Kamiya, and H. Hosono, The journal of physical chemistry letters **6**, 4966 (2015).

[37]S. B. Dawes, A. S. Ellaboudy, and J. L. Dye, J. Am. Chem. Soc. **109**, 3508 (1987).

[38]R. Huang, M. Faber, K. Moeggenborg, D. Ward, and J. Dye, (1988).

[39]Z. Li, J. Yang, J. G. Hou, and Q. Zhu, J. Am. Chem. Soc. **125**, 6050 (2003).

[40]J. Medvedeva and A. Freeman, Appl. Phys. Lett. **85**, 955 (2004).

[41]J. Medvedeva, A. Freeman, M. Bertoni, and T. Mason, Phys. Rev. Lett. **93**, 016408 (2004).

[42]I. G. Ryabinkin and V. N. Staroverov, Phys. Chem. Chem. Phys. **13**, 21615 (2011).

[43]S. Guan, S. A. Yang, L. Zhu, J. Hu, and Y. Yao, Scientific reports **5** (2015).

[44]Y. He, Journal of Alloys and Compounds **654**, 180 (2016).

[45]K. Lee, S. W. Kim, Y. Toda, S. Matsuishi, and H. Hosono, Nature **494**, 336 (2013).

[46]X. Zhang, Z. Xiao, H. Lei, Y. Toda, S. Matsuishi, T. Kamiya, S. Ueda, and H. Hosono, Chemistry of Materials **26**, 6638 (2014).

[47]T. Inoshita, S. Jeong, N. Hamada, and H. Hosono, Physical Review X **4**, 031023 (2014).

[48]A. S. Ichimura, J. L. Dye, M. A. Camblor, and L. A. Villaescusa, J Am. Chem. Soc. **124**, 1170 (2002).

[49]V. Petkov, S. Billinge, T. Vogt, A. Ichimura, and J. Dye, Phys. Rev. Lett.G **89**, 075502 (2002).

[50]J. L. Dye, Science **301**, 607 (2003).

[51]Y. Li, Z.-R. Li, D. Wu, R.-Y. Li, X.-Y. Hao, and C.-C. Sun, J. Phys. Chem. B **108**, 3145 (2004).

[52]W. Chen, Z.-R. Li, D. Wu, F.-L. Gu, X.-Y. Hao, B.-Q. Wang, R.-J. Li, and C.-C. Sun, J. Chem. Phys. **121**, 10489 (2004).

[53]W. Chen, Z.-R. Li, D. Wu, Y. Li, C.-C. Sun, and F. L. Gu, J. Am. Chem. Soc. **127**, 10977 (2005).

[54]W. Chen, Z.-R. Li, D. Wu, Y. Li, C.-C. Sun, F. L. Gu, and Y. Aoki, J. Am. Chem. Soc. **128**, 1072 (2006).

[55]Y.-Q. Jing, Z.-R. Li, D. Wu, Y. Li, B.-Q. Wang, F. L. Gu, and Y. Aoki, ChemPhysChem **7**, 1759 (2006).

[56]F.-F. Wang, Z.-R. Li, D. Wu, B.-Q. Wang, Y. Li, Z.-J. Li, W. Chen, G.-T. Yu, F. L. Gu, and Y. Aoki, J. Phys. Chem. B **112**, 1090 (2008).

[57]F. Ma, Z.-R. Li, H.-L. Xu, Z.-J. Li, Z.-S. Li, Y. Aoki, and F. L. Gu, J. Phys. Chem. A **112**, 11462 (2008).

[58]S. Muhammad, H. Xu, Y. Liao, Y. Kan, and Z. Su, J. Am. Chem. Soc. **131**, 11833 (2009).

[59]Z.-J. Li, Z.-R. Li, F.-F. Wang, C. Luo, F. Ma, D. Wu, Q. Wang, and X.-R. Huang, J. Phys. Chem. A **113**, 2961 (2009).

[60]Z.-B. Liu, Z.-J. Zhou, Y. Li, Z.-R. Li, R. Wang, Q.-Z. Li, Y. Li, F.-Y. Jia, Y.-F. Wang, Z.-J. Li, *et al.*, Phys. Chem. Chem. Phys. **12**, 10562 (2010).

[61]H.-L. Xu, F.-F. Wang, W. Chen, and G.-T. Yu, International Journal of Quantum Chemistry **111**, 3174 (2011).

[62]H.-L. Xu, S.-L. Sun, S. Muhammad, and Z.-M. Su, Theoretical Chemistry Accounts **128**, 241 (2011).

[63]Z.-J. Zhou, H. Li, X.-R. Huang, Z.-J. Wu, F. Ma, and Z.-R. Li, Computational and Theoretical Chemistry **1023**, 99 (2013).

[64]A. K. Srivastava and N. Misra, New Journal of Chemistry **38**, 2890 (2014).

[65]W.-M. Sun, L.-T. Fan, Y. Li, J.-Y. Liu, D. Wu, and Z.-R. Li, Inorganic chemistry **53**, 6170 (2014).

[66]W.-M. Sun, D. Wu, Y. Li, and Z.-R. Li, Dalton Transactions **43**, 486 (2014).

[67]V. Postils, M. Garcia-Borràs, M. Solà, J. M. Luis, and E. Matito, Chemical Communications **51**, 4865 (2015).

[68]A. Kumar and S. R. Gadre, Phys. Chem. Chem. Phys. **17**, 15030 (2015).

[69]R.-L. Zhong, H.-L. Xu, Z.-R. Li, and Z.-M. Su, J. Phys. Chem. Lett. **6**, 612 (2015).

[70]B. G. Janesko, G. Scalmani, and M. J. Frisch, Journal of chemical theory and computation (2015).

[71]I. G. Ryabinkin and V. N. Staroverov, Phys. Rev. A **82**, 022505 (2010).

[72]I. G. Ryabinkin and V. N. Staroverov, Physical Review A **81**, 032509 (2010).

[73]P. E. Blöchl, Physical Review B **50**, 17953 (1994).

[74]P. Giannozzi, S. Baroni, N. Bonini, M. Calandra, R. Car, C. Cavazzoni, D. Ceresoli, G. L. Chiarotti, M. Cococcioni, I. Dabo, *et al.*, Journal of Physics: Condensed Matter **21**, 395502 (2009).

[75]J. P. Perdew, K. Burke, and M. Ernzerhof, Physical review letters **77**, 3865 (1996).

[76]N. Marzari, D. Vanderbilt, A. De Vita, and M. Payne, Physical review letters **82**, 3296 (1999).

[77]A. O. de-la Roza, M. Blanco, A. M. Pend?s, and V. Lua?a, Computer Physics Communications **180**, 157 (2009).

[78]A. O. de-la Roza, E. R. Johnson, and V. Lua?a, Computer Physics Communications **185**, 1007 (2014).

[79]M. Yu and D. R. Trinkle, J. Chem. Phys. **134** (2011).

[80]F. H. Allen, Acta Crystallographica Section B: Structural Science **58**, 380 (2002).

[81]A. J. Cohen, P. Mori-Sánchez, and W. Yang, J. Chem. Phys. **129**, 121104 (2008).

[82]A. D. Becke, The Journal of chemical physics **138**, 161101 (2013).

[83]W. D. Laidig, P. Saxe, and R. J. Bartlett, The Journal of chemical physics **86**, 887 (1987).

[84]F. Neese, Journal of Physics and Chemistry of Solids **65**, 781 (2004).

[85]K. Andersson, P. A. Malmqvist, B. O. Roos, A. J. Sadlej, and K. Wolinski, J. Phys. Chem. **94**, 5483 (1990).

[86]K. Andersson, P.-Å. Malmqvist, and B. O. Roos, J. Chem. Phys. **96**, 1218 (1992).

[87]K. Andersson, Theoretica chimica acta **91**, 31 (1995).

[88]K. Yamaguchi, F. Jensen, A. Dorigo, and K. Houk, Chemical physics letters **149**, 537 (1988).

[89]L. Noodleman, C. Peng, D. Case, and J.-M. Mouesca, Coordination Chemistry Reviews **144**, 199 (1995).

[90]Y. Kitagawa, T. Saito, M. Ito, M. Shoji, K. Koizumi, S. Yamanaka, T. Kawakami, M. Okumura, and K. Yamaguchi, Chem. Phys. Lett. **442**, 445 (2007).

[91]H. P. Hratchian, The Journal of chemical physics **138**, 101101 (2013).

[92]L. M. Thompson and H. P. Hratchian, The Journal of chemical physics **141**, 034108 (2014).

[93]L. M. Thompson and H. P. Hratchian, The Journal of chemical physics **142**, 054106 (2015).

[94]M. A. Spackman and E. N. Maslen, The Journal of Physical Chemistry **90**, 2020 (1986).

[95]E. Johnson, S. Keinan, P. Mori-Sánchez, J. . Contreras-García, A. Cohen, and W. Yang, J. Am. Chem. Soc. **132**, 6498 (2010).

[96]J. Contreras-Garca, E. R. Johnson, S. Keinan, R. Chaudret, J.-P. Piquemal, D. N. Beratan, and W. Yang, J. Chem. Theor. Comput. **7**, 625 (2011).

[97]A. Otero-de-la Roza, E. R. Johnson, and J. Contreras-García, Phys. Chem. Chem. Phys. **14**, 12165 (2012).

[98]E. R. Johnson, S. Keinan, P. Mori-Sánchez, J. Contreras-García, A. J. Cohen, and W. Yang, J. Am. Chem. Soc. **132**, 6498 (2010).

[99]A. Otero de la Roza, E. R. Johnson, and J. Contreras-Garcia, Phys. Chem. Chem. Phys. **14**, 12165 (2012).

[100]F. Uhlig, O. Marsalek, and P. Jungwirth, J. Phys. Chem. Lett. **3**, 3071 (2012).

[101]B. G. Janesko, G. Scalmani, and M. J. Frisch, Physical Chemistry Chemical Physics **17**, 18305 (2015).

[102]E. R. Johnson, A. Otero-de-la Roza, and S. G. Dale, J. Chem. Phys. **139**, 184116 (2013).

[103]S. G. Dale and E. R. Johnson, J, Chem. Phys. **143**, 184112 (2015).

[104]T. Soda, Y. Kitagawa, T. Onishi, Y. Takano, Y. Shigeta, H. Nagao, Y. Yoshioka, and K. Yamaguchi, Chem. Phys. Lett. **319**, 223 (2000).

[105]J. L. Sonnenberg, H. B. Schlegel, and H. P. Hratchian, Encyclopedia of Inorganic Chemistry (2009).

[106]A. Otero-de-la Roza and E. R. Johnson, J. Chem. Phys. **138** (2013).

[107]S. E. Wheeler, Wiley Interdisciplinary Reviews: Computational Molecular Science **2**, 204 (2012).